Self-diffusion, conductivity, and long-wavelength plasma oscillations in strongly coupled two-component plasmas

L. Sjögren* and J. P. Hansen
Laboratoire de Physique Theorique des Liquides,† Universite Pierre et Marie Curie, 4 Place Jussieu, 75230 Paris Cedex 05, France

E. L. Pollock
Lawrence Livermore National Laboratory, P.O. Box 808, Livermore, California 94550
(Received 30 March 1981)

The autocorrelation functions of the microscopic electric current $J(t)$ and the electron velocity $Z_2(t)$ are calculated for strongly coupled, semiclassical two-component plasmas. The corresponding memory functions are expressed in terms of mode-coupling integrals involving density- and energy-correlation function in the framework of a microscopic kinetic theory which preserves the exact statics. Through a sequence of well-defined approximations, the expressions for the memory functions are made self-consistent, the resulting equations are solved iteratively with the interaction potentials, and the static-partial-structure factors as the only input. The theory is then applied to weakly degenerate hydrogen and carbon plasmas for values of the plasma parameter of order 1. The resulting correlational functions $J(t)$ and $Z_2(t)$ and their integrals, the electrical conductivity, and the electron self-diffusion constant, agree reasonably well with the "molecular-dynamics" data of Hansen and McDonald and with additional simulation results presented here. The "long-time tail" in $J(t)$ observed in the simulations is interpreted in terms of mode-coupling effects. The damping and frequency shift of the plasmon peak in the dynamical charge-fluctuation spectrum are explicitly evaluated in the long-wavelength limit; the frequency shift above the plasma frequency is shown to be nonnegligible for strong coupling.

I. INTRODUCTION

The statistical mechanics of highly compressed, fully ionized plasmas is attracting an increasing amount of attention, particularly in connection with the physics of laser fusion and of steller interiors.[1,2] Extensive information on the microscopic dynamics of a strongly coupled two-component (TCP) hydrogen plasma has recently been gained from "molecular-dynamics" (MD) simulations.[3,4] From an analysis of the time-dependent equilibrium correlation functions generated in these simulations it was concluded that: (a) the frequency of the plasmon mode in the long-wavelength limit is shifted by a sizable amount above the electron plasma frequency, due to ion-electron collisions (resistivity); (b) a marked "long-time tail" occurs in the electric current autocorrelation function (ACF), $J(t)$, which leads to a considerable enhancement of the electrical conductivity σ over the value expected on the basis of electron self-diffusion. In a subsequent paper,[5] a first attempt was made to estimate σ theoretically and a divergence free generalization of the standard Spitzer formula[6] for σ was derived. In this paper we extend the latter analysis and present a microscopic kinetic theory for the calculation of the time dependence of the electric current ACF $J(t)$, and of the electron velocity ACF $Z_2(t)$. To test some of our theoretical results, we have performed additional MD simulations which complement those contained in Refs. 3 and 4.

We consider a fully ionized plasma of ions (1) and electrons (2), of mass m_a and charge $Z_a e$ ($a=1,2$), respectively. From the partial number density $n_a = N_a/V$ (where V denotes the volume of the system) we define the total number density

$$n = \sum_a n_a ,$$

and the total mass density

$$\rho = \sum_a \rho_a = \sum_a n_a m_a .$$

Owing to overall charge neutrality, the total charge density vanishes:

$$\sum_a Z_a n_a = 0 . \tag{1.1}$$

For the special case of a hydrogen plasma, we have $Z_1 = -Z_2 = 1$, which implies that $n_1 = n_2$. More generally, the ionic charge is $Z_1 = Z$ and then $n_2 = Z n_1$.

To characterize an equilibrium state of the plasma, we introduce the usual dimensionless parameters Γ and r_s, where

$$\Gamma = \frac{\beta e^2}{a} \tag{1.2}$$

is the plasma parameter defined in terms of the

inverse temperature $\beta = 1/k_B T$ and of the mean inter-electronic spacing (or "electron sphere radius") $a = (\frac{3}{4}\pi n_2)^{1/3}$. r_s is the ratio of this spacing over the Bohr radius $a_0 = \hbar^2/m_2 e^2$,

$$r_s = \frac{a}{a_0}. \tag{1.3}$$

The strong-coupling regime investigated in this work corresponds to $\Gamma \gtrsim 1$.

The microscopic dynamics of the plasma typically involve two very distinct time scales, due to the large ion to electron mass ratio; these time scales are characterized by the electron and ion plasma frequencies

$$\omega_{pa} = \left(\frac{4\pi Z_a^2 e^2 n_a}{m_a}\right)^{1/2}.$$

We shall restrict ourselves to a range of temperatures and densities such that the electron de Broglie thermal wavelength is shorter than the inter-particle spacing a. For such a semiclassical plasma, quantum diffraction effects, which come into play only at short distances, can approximately be accounted for by the use of effective pair potentials of the form[7]

$$v^{ab}(r) = Z_a Z_b \frac{e^2}{r}(1 - e^{-r/\lambda_{ab}}), \quad a, b = 1, 2 \tag{1.4}$$

where $\lambda_{ab} = \hbar(\beta/2\pi\mu_{ab})^{1/2}$ is the de Broglie thermal wavelength for the pair (a, b), and μ_{ab} is the reduced mass of the pair. Note that the potential (1.4) prevents the classical collapse of ion-electron pairs. Moreover, when the temperature becomes of the order of the electron Fermi temperature T_F, electron degeneracy effects become important, and these are approximately taken into account by adding a symmetry term to the electron-electron interaction[8]

$$v_s^{22}(r) = \frac{\ln 2}{\beta}\exp[-r^2/(\pi \ln 2 \lambda_{22}^2)]. \tag{1.5}$$

Note that the MD simulations of Hansen and McDonald[3,4] were carried out with the effective pair potentials (1.4), i.e., without including the additional electron-electron repulsion (1.5) due to the Pauli principle. In order to test the sensitivity of the various correlation functions and transport coefficients with respect to electron symmetry effects, we have carried out the calculations presented in this paper for a hydrogen plasma both with and without the inclusion of the term (1.5) in the effective pair potential. We have also extended the calculations to the case of a fully ionized carbon plasma ($Z = 6$).

The outline of the paper is the following: In Sec. II we introduce various definitions and formal expressions for the memory function of $J(t)$ and $Z_2(t)$ in a kinetic theoretical formulation. A succession of approximations, leading to a tractable expression for these memory functions, is described in Sec. III. Section IV is devoted to an analysis of the weak-coupling limit of the theory. Numerical results, based on the approximation scheme outlined in Sec. III, are compared in Sec. V to MD simulation data and discussed in the concluding Sec. VI.

II. FORMAL EXPRESSIONS FOR THE MEMORY FUNCTION

Our analysis is based on the kinetic theory of equilibrium fluctuations which has been developed in connection with simple classical liquids,[9] two-component neutral fluids[10] and plasmas,[11] and we refer the reader to these references for details.

The basic quantities of interest in this paper are the autocorrelation function (ACF) $J(t)$ of the total microscopic electric current[12]

$$J(t) = \frac{\langle \vec{j}(t) \cdot \vec{j}(0) \rangle}{\langle j^2(0) \rangle}, \tag{2.1}$$

where

$$\vec{j}(t) = \sum_a \sum_{i=1}^{N_a} Z_a \vec{v}_{ia}(t) \tag{2.2}$$

and the velocity ACF of species a

$$Z_a(t) = \frac{\langle \vec{v}_{ia}(t) \cdot \vec{v}_{ia}(0) \rangle}{\langle v_{ia}^2(0) \rangle}, \quad a = 1, 2. \tag{2.3}$$

In Eqs. (2.2) and (2.3), $\vec{v}_{ia}(t)$ denotes the velocity at time t of particle i belonging to species a.

The memory functions associated with $J(t)$ and $Z_a(t)$ are defined in terms of the Laplace transforms by

$$J(z) = [z + M_J(z)]^{-1}, \tag{2.4}$$

$$Z_a(z) = [z + M_a(z)]^{-1}, \tag{2.5}$$

where

$$J(z) = \int_0^\infty dt\, e^{-zt} J(t) \tag{2.6}$$

denotes the Laplace transform of $J(t)$, etc. The frequency-dependent (ac) conductivity is simply related to $J(z)$ by

$$\sigma(z) = \frac{\omega_p^2}{4\pi} J(z), \tag{2.7}$$

where $\omega_p^2 = \omega_{p1}^2 + \omega_{p2}^2$ is the square of the total plasma frequency.

Explicit expressions for the memory functions can be obtained by considering the microscopic phase-space correlation functions

$$C^{ab}(1t;2t') = \langle \delta f_1^a(1t)\, \delta f_1^b(2t') \rangle, \tag{2.8}$$

and correspondingly for the self-motion

$$C^{sa}(1t;2t') = \langle \delta f_1^{sa}(1t)\, \delta f_1^{sa}(2t') \rangle . \tag{2.9}$$

Here δf_1^a and δf_1^{sa} denote the fluctuations in the microscopic phase-space distribution functions:

$$\delta f_1^{sa}(1t) = (N_a)^{1/2} \delta(1 - q_{ia}(t)) - \frac{(N_a)^{1/2}}{V} \phi_M^a(p_1) , \tag{2.10a}$$

$$\delta f_1^a(1t) = \sum_{i=1}^{Na} \delta(1 - q_{ia}(t)) - n_a \phi_M^a(p_1) , \tag{2.10b}$$

and $q_{ia}(t) = (\vec{r}_{ia}(t), \vec{P}_{ia}(t))$ is the six-dimensional phase-space variable associated with particle i of species a; ϕ_M^a denotes the Maxwellian distribution

$$\phi_M^a(p) = \left(\frac{\beta}{2\pi m_a}\right)^{3/2} \exp\left(-\frac{\beta p^2}{2m_a}\right). \tag{2.11}$$

It is customary to eliminate the momentum dependence of the phase-space correlation functions by defining their matrix elements with respect to a complete set of Hermite polynomials $H_\mu^a(p)$ as follows:

$$C_{\mu\nu}^{ab}(\vec{k}z) = \int d\vec{p}_1 \int d\vec{p}_2 H_\mu^a(\vec{p}_1) C^{ab}(\vec{k}z; \vec{p}_1\vec{p}_2) H_\nu^b(\vec{p}_2) , \tag{2.12}$$

where the $H_\mu^a(p)$ are orthornormalized according to

$$\int d\vec{p}\, H_\mu^a(\vec{p}) H_\nu^a(\vec{p}) n_a \phi_M^a(p) = \delta_{\mu\nu} . \tag{2.13}$$

The phase-space correlation functions $C_{\mu\nu}^{ab}(kz)$ can be expressed in terms of memory functions $\Gamma_{\mu\nu}^{ab}(kz)$ by[9,10]

$$zC_{\mu\nu}^{ab}(\vec{k}z) - \sum_{a_1} \sum_{\lambda} \Omega_{\mu\lambda}^{aa_1}(\vec{k}z) C_{\lambda\nu}^{a_1 b}(\vec{k}z) + \sum_{a_1} \sum_{\lambda} \Gamma_{\mu\lambda}^{aa_1}(\vec{k}z) C_{\lambda\nu}^{a_1 b}(\vec{k}z) = \tilde{C}_{\mu\nu}^{ab}(\vec{k}) \tag{2.14}$$

and similarly for C^{sa}. $\tilde{C}$ denotes the initial value of C. Ω is explicitly known in terms of static correlation functions.

The first five polynomials $H_\mu^a(p)$, $(\mu = 0, \ldots, 4)$ are given by

$$H_\mu^a(\vec{p}) = \left\{ (n_a)^{-1/2}, (\beta/\rho_a)p^x, (\beta/\rho_a)p^x, (\beta/\rho_a)p^y, (6n_a)^{-1/2}\left(\frac{\beta}{m_a}p^2 - 3\right) \right\} , \tag{2.15}$$

and correspond to the density, momentum, and kinetic energy fluctuations of species a, respectively. The wave vector k is chosen to be parallel to the z direction, and the element $\mu = 1$ is therefore associated with the longitudinal current. In addition to the five elements in Eq. (2.15), we shall need the element $H_Q^a(p)$ representing the longitudinal energy current:

$$H_Q^a(\vec{p}) = \left(\frac{\beta}{10\rho_a}\right)^{1/2} p^x \left(\frac{\beta}{m_a}p^2 - 5\right) . \tag{2.16}$$

$H_Q^a(\vec{p})$ coincides in fact with the so-called "second-order Sonine polynomial" from the conventional set of polynomials at $\vec{k} = 0$.[13] Taking $\mu = \nu = 0$ in Eq. (2.12) we generate the partial dynamical density correlation functions and, by suitable linear combination, the charge-charge, charge-mass, and mass-mass dynamical structure factors C_{ZZ}, C_{MZ}, and C_{MM}; for instance,

$$C_{ZZ}(kz) = \left(\sum_a Z_a^2 n_a\right)^{-1} \sum_{ab} \sum Z_a Z_b (n_a n_b)^{1/2} C_{00}^{ab}(kz) . \tag{2.17}$$

The dielectric function $\epsilon(kz)$ is related to the charge-charge response function $X_{ZZ}(kz)$, which, in turn, is given in terms of $C_{ZZ}(kz)$ via the fluctuation-dissipation theorem

$$\frac{1}{\epsilon(kz)} = 1 + \frac{4\pi e^2}{k^2} X_{ZZ}(k,z) = 1 + \frac{k_D^2}{k^2}[zC_{ZZ}(kz) - S_{ZZ}(k)] , \tag{2.18}$$

where $S_{ZZ}(k) \equiv \tilde{C}_{ZZ}(k)$ is the static charge-charge structure factor, and

$$k_D^2 = 4\pi\beta e^2 \sum_a Z_a^2 n_a$$

is the square of the Debye wave number. The dielectric function is also related to the nonlocal conductivity $\sigma(kz)$ via[12]

$$\epsilon(kz) = 1 + \frac{4\pi}{z}\sigma(kz) . \tag{2.19}$$

To derive an explicit expression of the memory function M_J in terms of the Γ^{ab} introduced in Eq. (2.14) we now proceed as follows. From Eqs. (2.18) and (2.19) we obtain a relation between $\sigma(z) = \lim_{k\to 0}\sigma(kz)$ and the long-wavelength limit of $C_{ZZ}(kz)$. To extract an expression for the latter function from Eq. (2.14) we proceed along the conventional lines proposed by Forster and Martin[14] by introducing a hydrodynamic projection operator, which projects into the subspace spanned by the five hydrodynamic momentum states of Eq. (2.15). The details of this procedure in the case of a two-component plasma can be found in the papers by Baus,[11] leading to the final result

$$\lim_{k\to 0}\frac{k_D^2}{k^2}[zC_{ZZ}(kz) - S_{ZZ}(k)] = -\frac{\omega_p^2}{z^2 + \omega_p^2 + z[\nu_l^{11}(z) + \nu_l^{22}(z)]} , \tag{2.20}$$

where

$$\nu_l^{aa}(z) = \Gamma_{11}^{aa}(z) - \sum_{a_1 a_2}\sum_{\lambda,\eta>4}\Gamma_{1\lambda}^{aa_1}(z) R_{\lambda\eta}^{a_1 a_2}(z)\Gamma_{\eta 1}^{a_2 a}(z) , \tag{2.21}$$

with

$$\sum_{a_1}\sum_{\lambda>4}[z\delta_{aa_1}\delta_{\mu\lambda} + \Gamma_{\mu\lambda}^{aa_1}(z)]R_{\lambda\nu}^{a_1 b}(z) = \delta_{ab}\delta_{\mu\nu}, \quad \mu,\nu>4 \tag{2.22}$$

and

$$\Gamma_{\mu\nu}^{ab}(z) = \lim_{k\to 0}\Gamma_{\mu\nu}^{ab}(\vec{k}z) .$$

Combining Eqs. (2.18)–(2.20) we then obtain

$$\sigma(z) = \frac{\omega_p^2}{4\pi}\frac{1}{z + \nu_l^{11}(z) + \nu_l^{22}(z)} \tag{2.23}$$

and, by identification with Eqs. (2.4) and (2.7), the desired exact expression for $M_J(z)$ reads

$$M_J(z) = \nu_l^{11}(z) + \nu_l^{22}(z) = \frac{\rho}{\rho_1}\nu_l^{22}(z) . \tag{2.24}$$

The last step follows from momentum conservation, which leads to [11]

$$\sum_a (\rho_a)^{1/2}\Gamma_{1\lambda}^{ab}(z) = \sum_b \Gamma_{\lambda 1}^{ab}(\rho_b)^{1/2} \equiv 0 . \tag{2.25}$$

III. APPROXIMATIONS

As it stands, the exact expression (2.21)–(2.24) for $M_J(z)$ is untractable, and we are led to make a succession of four well-defined approximations which allow an explicit, self-consistent calculation of the memory functions $M_J(z)$ and $M_4(z)$. We introduce and discuss these approximations one by one.

A. Two Sonine polynomial approximation

Returning to Eq. (2.21) we see that the second term on the right-hand side (rhs) involves a double sum over all nonhydrodynamic states λ, $\eta>4$. In Ref. 5 this term was neglected altogether (except for a factor of 1.93 in the resulting expression for σ), leading immediately to an explicit expression of $M_J(t)$ in terms of the density correlation functions $C_{00}^{ab}(k,t)$. It is known from previous calculations based on Boltzmann-type or Fokker-Planck equations,[15-19] that for a plasma in the weak-coupling limit ($\Gamma \ll 1$), this term can give a contribution comparable to the first term Γ_{11}^{aa}. Moreover, these studies have shown that the sum in Eq. (2.21) is practically exhausted by the first nonvanishing element, which involves precisely the nonhydrodynamic element H_Q^a introduced in Eq. (2.16). Restricting the sum to this term corresponds to the second-order Sonine polynomial approximation which, after solving for R_{QQ}^{ab} from Eq. (2.22), yields the following expression for $\nu_l^{22}(z)$:

$$\nu_l^{22}(z) = \Gamma_{11}^{22}(z) - \{(\rho_1/\rho_2)[\Gamma_{1Q}^{11}(z)]^2[z + \Gamma_{QQ}^{22}(z)] + 2(\rho_1/\rho_2)^{1/2}\Gamma_{1Q}^{11}(z)\Gamma_{1Q}^{22}(z)\Gamma_{QQ}^{12}(z) + [\Gamma_{1Q}^{22}(z)]^2[z + \Gamma_{QQ}^{11}(z)]\}/\Delta(z) , \tag{3.1}$$

where

$$\Delta(z) = [z + \Gamma_{QQ}^{11}(z)][z + \Gamma_{QQ}^{22}(z)] - [\Gamma_{QQ}^{12}(z)]^2 . \tag{3.2}$$

To derive Eq. (3.1), use was made of Eq. (2.25) and of the symmetry of the memory function matrix

$$\Gamma_{\mu\nu}^{ab}(z) = -\Gamma_{\nu\mu}^{ba}(-z) . \tag{3.3}$$

Consideration of the dependence of the matrix elements $\Gamma_{\mu\nu}^{ab}$ on the mass ratio m_2/m_1 will in fact lead to a considerable simplification of the expression (3.1) for ν_l^{22} for a plasma, where $m_2/m_1 \ll 1$. For more generality we keep at pre-

sent the full expression (3.1) which could also be used for an analysis of electrical conductivity in molten salts, where $m_1/m_2 \simeq 1$.[20,12]

The analysis for the self-motion is similar to the previous analysis of electrical conductivity, but considerably simpler, and the resulting memory function reads in the two Sonine polynomial approximation

$$M_a(z) = \Gamma^{sa}_{11}(z) - \frac{[\Gamma^{sa}_{1Q}(z)]^2}{z + \Gamma^{sa}_{QQ}(z)}, \tag{3.4}$$

where Γ^{sa} denotes the phase-space memory function matrix for the self-motion. The remaining task is to calculate explicitly the matrix elements of Γ^{ab} and Γ^{sa} appearing in Eqs. (3.1), (3.2), and (3.4).

B. Disconnected approximation

Exact expressions for the phase-space memory functions Γ^{ab} (and Γ^{sa}) are known in the form[9,10]

$$\Gamma^{ab}_{\mu\nu}(t) = \frac{1}{V}\sum_{a_1}\sum_{a_2}\int d1\cdots d4\ \vec{\nabla}_{\vec{p}_1} H^a_\mu(\vec{p}_1)\cdot\vec{\nabla}_{\vec{r}_1} v^{aa_1}(\vec{r}_1-\vec{r}_2)\, G^{aa_1;ba_2}(12;34t)\,\vec{\nabla}_{\vec{r}_3} v^{ba_2}(\vec{r}_3-\vec{r}_4)\cdot\vec{\nabla}_{\vec{p}_3} H^b_\nu(\vec{p}_3). \tag{3.5}$$

The four-point function G describes the correlated motion of two particles in the plasma. The simplest approximation for this function is a straightforward factorization ("disconnected approximation"[9]), i.e., $G \simeq G_D$, where

$$G_D^{aa_1;ba_2}(12;34t) = C^{ab}(13t)\,C^{a_1a_2}(24t) + C^{aa_2}(14t)\,C^{ab_1}(23t). \tag{3.6}$$

Physically, this factorization describes a situation where the two particles move independently of each other, but interact with the other particles in the surrounding medium. The approximation (3.6) will, however, destroy the exact initial value of $\Gamma^{ab}(t)$ in Eq. (3.5), and consequently of $M_J(t)$; we expect that this failure might introduce large errors for a strongly coupled system. In Appendix A we sketch a procedure[21,22] which preserves the exact value of $M_J(t=0)$ and satisfies the symmetry relation (3.3). The final result for Γ^{ab} reads

$$\Gamma^{ab}_{\mu\nu}(t) = -\frac{1}{2\beta}\sum_{a_1}\sum_{a_2}(n_{a_1}n_{a_2})^{1/2}\int\frac{d\vec{k}'}{(2\pi)^3}\,k'^{\alpha}k'^{\beta}[v^{aa_1}(k')c^{ba_2}(k')+c^{aa_1}(k')v^{ba_2}(k')]$$
$$\times[C^{qb}_{\lambda\eta}(-\vec{k}',t)\,C^{a_1a_2}_{00}(\vec{k}'t) - C^{aa_2}_{\lambda 0}(-\vec{k}',t)\,C^{a_1b}_{0\eta}(\vec{k}'t)]$$
$$\times\int d\vec{p}_1\int d\vec{p}_2\ \nabla^{\alpha}_{\vec{p}_1} H^a_\mu(\vec{p}_1)\,H^a_\lambda(\vec{p}_1)\,\nabla^{\beta}_{\vec{p}_2} H^b_\nu(\vec{p}_2)\,H^b_\eta(\vec{p}_2)\,n_a n_b\,\phi^a_M(p_1)\,\phi^b_M(p_2). \tag{3.7}$$

In Eq. (3.7) the $c^{ab}(k)$ are the partial direct-correlation functions, and summation over repeated Greek indices is implied, a convention which we henceforth adopt. Note that to derive Eq. (3.7), the correlation functions have been expanded in the complete set of momentum states $H^a_\mu(\vec{p})$. Effectively what we have done to derive Eq. (3.7) from Eq. (3.5) is to replace one of the bare potentials v by the effective potential $(-c/\beta)$.[23] In the weak-coupling limit this replacement has no effect since the two potentials are then identical, while for stronger coupling we expect the static correlations inherent in c to play an important role. From Eq. (3.7) we obtain for the matrix element $\mu=\nu=1$

$$\Gamma^{22}_{11}(t) = -\frac{n_1}{m_2}\frac{1}{6\pi^2}\int_0^\infty dk'\,k'^4 v^{12}(k')c^{12}(k') \times[C^{11}_{00}(k't)C^{22}_{00}(k't) - C^{21}_{00}(k't)C^{12}_{00}(k't)]. \tag{3.8}$$

Using the Ornstein-Zernike relation

$$(n_1n_2)^{1/2}c^{12}(k) = \frac{S^{12}(k)}{[S^{11}(k)S^{22}(k) - S^{21}(k)S^{12}(k)]}, \tag{3.9}$$

we find for $t=0$

$$\Gamma^{22}_{11}(t=0) = -\frac{n_1}{m_2}(n_1n_2)^{-1/2}\frac{1}{6\pi^2}\int_0^\infty dk'k'^4 v^{12}(k')\,S^{12}(k') = \frac{n_1}{3m_2}\int d\vec{r}[g^{12}(r)-1]\nabla^2 v^{12}(r), \tag{3.10}$$

where $g^{ab}(r)$ denotes the partial-pair distribution function between species a and b, and $S^{ab}(k)$ the corresponding partial structure factor.

From Eqs. (2.24) and (3.1) it is readily checked that Eq. (3.10) implies the known exact initial value of $M_J(t)$.[4] Indeed Γ^{ab}_{1Q} starts as t^2, i.e., behaves as $1/z^3$ for large z, and the second term in Eq. (3.1) therefore starts as $1/z$,[7] i.e., as t^6 for short times; hence, in the $t\to 0$ limit only $\Gamma^{22}_{11}(t)$ contributes to $M_J(t)$.

In Eq. (3.8) we have expressed Γ_{11}^{22} in terms of the partial-density correlation functions. Alternatively, we could introduce linear combinations of these, as in Eq. (2.17), and express Γ_{11}^{22} in terms of the total mass and charge fluctuations. This linear transformation gives

$$C_{00}^{11}(kt)C_{00}^{22}(kt) - C_{00}^{21}(kt)\,C_{00}^{12}(kt) = \frac{n}{\rho}[C_{MM}(kt)\,C_{ZZ}(kt) - C_{ZM}(kt)\,C_{MZ}(kt)]\,, \quad (3.11)$$

where C_{ZZ}, C_{MM}, and $C_{MZ} = C_{ZM}$ denote the charge-charge, mass-mass, and mass-charge correlation functions, respectively. Equations (3.8) and (3.11) indicate how the time dependence of $\Gamma_{11}^{22}(t)$ or $J(t)$ is built up from the coupling to microscopic charge and mass fluctuations. The former give rise to a microscopic electric field and thereby a corresponding electric current, while the latter represent an electrostrictive effect.[24] Note that in the one Sonine polynomial approximation, $M_J(t)$ reduces to $\Gamma_{11}^{22}(t)\,\rho/\rho_1$, so that Eq. (3.8) is precisely the expression for $M_J(t)$ derived in Ref. 5. In the two Sonine polynomial approximation, we must evaluate the other matrix elements entering in the second term on the rhs of Eq. (3.1). Proceeding as for $\Gamma_{11}^{22}(t)$, we find

$$\Gamma_{1Q}^{ab}(t) = -\frac{1}{2(m_a m_b)^{1/2}}\sum_{a_1}\sum_{a_2}(n_{a_1}n_{a_2})^{1/2}\int\frac{d\vec{k}'}{(2\pi)^3}\,k'^{\alpha}k'^{\beta}[v^{aa_1}(k')c^{ba_2}(k') + c^{aa_1}(k')v^{ba_2}(k')] \times [C_{0\eta}^{ab}(-\vec{k}', t)\,C_{00}^{a_1a_2}(\vec{k}'t) - C_{00}^{aa_2}(\vec{k}'t)\,C_{00}^{a_1b}(\vec{k}'t)][(\tfrac{3}{5})^{1/2}\delta_{\beta\alpha}\,\delta_{\eta 4} + (\tfrac{2}{5})^{1/2}\delta_{\eta\beta}]. \quad (3.12)$$

This expression involves the correlation function C_{04}^{ab}, which couples to the kinetic energy fluctuations, and the correlation functions $C_{0\beta}^{ab}$ defined by

$$C_{0\beta}^{ab}(\vec{k}, t) = \int d\vec{p}_1 \int d\vec{p}_2 (n_a)^{-1/2} C^{ab}(\vec{k}\,t, \vec{p}_1\vec{p}_2)\left(\frac{\beta}{m_b}\,p_2^{\alpha}p_2^{\beta} - \delta_{\beta\alpha}\right) \quad (\beta = x, y, z). \quad (3.13)$$

The latter functions can in fact be written as linear combinations of C_{04}^{ab} and other nonhydrodynamic functions representing fluctuations in the kinetic stresses. Similarly, we find

$$\Gamma_{QQ}^{ab}(t) = -\frac{1}{2(m_a m_b)^{1/2}}\sum_{a_1}\sum_{a_2}(n_{a_1}n_{a_2})^{1/2}\int\frac{d\vec{k}'}{(2\pi)^3}\,k'^{\alpha}k'^{\beta}[v^{aa_1}(k')c^{ba_2}(k') + c^{aa_1}(k')v^{ba_2}(k')] \times [(\tfrac{3}{5})^{1/2}\delta_{\alpha\beta}\,\delta_{\lambda 4} + (\tfrac{2}{5})^{1/2}\delta_{\lambda\alpha}][C_{\lambda\eta}^{ab}(-\vec{k}', t)C_{00}^{a_1a_2}(\vec{k}'t) - C_{\lambda 0}^{aa_2}(-\vec{k}', t)C_{0\eta}^{a_1b}(\vec{k}'t)] \times [(\tfrac{3}{5})^{1/2}\delta_{\beta\alpha}\,\delta_{\eta 4} + (\tfrac{2}{5})^{1/2}\delta_{\eta\beta}], \quad (3.14)$$

which involves the correlation functions C_{44}^{ab}, $C_{4\beta}^{ab}$, and $C_{\alpha\beta}^{ab}$, where the latter are defined analogously to $C_{0\beta}^{ab}$ in Eq. (3.13), e.g.,

$$C_{\alpha\beta}^{ab}(\vec{k}t) = \int d\vec{p}_1 \int d\vec{p}_2\left(\frac{\beta}{m_a}\,p_1^{\alpha}p_1^{\beta} - \delta_{\alpha\beta}\right)C^{ab}(\vec{k}\,t; \vec{p}_1\vec{p}_2)\left(\frac{\beta}{m_b}\,p_2^{\alpha}p_2^{\beta} - \delta_{\beta\alpha}\right), \quad \alpha, \beta = x, y, z\,. \quad (3.15)$$

C. Effective-field approximation

In order to calculate the relevant matrix elements of Γ^{ab}, given by Eqs. (3.8), (3.12), and (3.14), we need explicit expressions for the various matrix elements of the phase-space correlation function C^{ab}. This can be achieved by assuming some simple form for Γ^{ab} in Eq. (2.14) and solving for C^{ab}. In this work we have used the "effective-field" (or "generalized mean field") approximation[25] to carry out this program; this approximation amounts to writing Γ^{ab} as the sum of its self and distinct parts

$$\Gamma_{\mu\nu}^{ab}(\vec{k}z) = \Gamma_{\mu\nu}^{sa}(\vec{k}z)\delta_{ab} + \Gamma_{\mu\nu}^{dab}(\vec{k}z)\,, \quad (3.16)$$

and then setting $\Gamma^d = 0$. The resulting expression for the correlation functions C^{ab} reads

$$C_{\mu\nu}^{ab}(\vec{k}z) - ik(\beta m_a)^{-1/2}\,C_{\mu 1}^{sa}(\vec{k}z) \times\sum_{a_1}(n_a n_{a_1})^{1/2}c^{aa_1}(k)\,C_{0\nu}^{a_1b}(\vec{k}z) = C_{\mu\lambda}^{sa}(\vec{k}z)\,\tilde{C}_{\lambda\nu}^{ab}(\vec{k})\,. \quad (3.17)$$

In this approximation the dynamics of C^{ab} is given in terms of the corresponding self-motion C^{sa} and

the static structure factors. The approximation (3.16)–(3.17) becomes exact in the limit of large k or weak coupling; in the latter, collisionless regime, it leads correctly to the correlation functions obtained from the linearized Vlasov equation. Moreover, comparison with the MD data on the hydrogen plasma shows that it gives a rather accurate description of the charge fluctuations.[4,27] It should be noted, however, that Eq. (3.17) violates conservation of momentum, and therefore fails to describe the mass fluctuations at small wave numbers.

D. Gaussian approximation for the self-motion

We now make a final approximation by adopting the so-called Gaussian approximation for the self-motion entering in Eq. (3.17); this approximation implies that all correlation functions can be expressed in terms of the velocity ACF's $Z_a(t)$. The Gaussian approximation has been tested for the one-component plasma,[26] where it was found to be very accurate; it also becomes exact in the weak-coupling limit. Within this approximation our expressions for Γ^{ab}_{1Q} and Γ^{ab}_{QQ} are greatly simplified, since the only independent correlation functions turn out to be C^{ab}_{00}, $C^{ab}_{04}=C^{ba}_{40}$ and C^{ab}_{44}. Details of the calculations are given in Appendix B. Using the results of this appendix we find

$$\Gamma^{ab}_{1Q}(t)=-(m_a m_b)^{-1/2}\sum_{a_2}(n_a n_{a_2})^{1/2}(\tfrac{3}{5})^{1/2}\frac{1}{4\pi^2}$$
$$\times\int_0^\infty dk'\,k'^4[v^{a\bar a}(k')\,c^{ba_2}(k')+c^{a\bar a}(k')v^{ba_2}(k')]$$
$$\times[C^{ab}_{04}(k't)\,C^{\bar a a_2}_{00}(k't)-C^{aa_2}_{00}(k't)\,C^{\bar a b}_{04}(k't)], \tag{3.18}$$

where $\bar a\neq a$, and

$$\Gamma^{ab}_{QQ}(t)=-(m_a m_b)^{-1/2}\sum_{a_1a_2}(n_{a_1}n_{a_2})^{1/2}\frac{9}{20\pi^2}$$
$$\times\int_0^\infty dk'\,k'^4[v^{aa_1}(k')\,c^{ba_2}(k')+c^{aa_1}(k')v^{ba_2}(k')]$$
$$\times[\bar C^{ab}_{44}(k't)\,C^{a_1a_2}_{00}(k't)-C^{aa_2}_{40}(k't)\,C^{a_1b}_{04}(k't)]\,, \tag{3.19}$$

with

$$\bar C^{ab}_{44}(kt)=C^{ab}_{44}(kt)-\left[\tfrac{4}{9}[Z_a(t)]^2+\tfrac{4}{27}\frac{k^2}{\beta m_a}Z_a(t)\left(\int_0^t dt'\,Z_a(t')\right)^2\right]C^{sa}_{00}(kt)\,\delta_{ab}\,. \tag{3.20}$$

Both Γ^{ab}_{1Q} and Γ^{ab}_{QQ} involve the coupling to the energy fluctuations via the correlation functions C^{ab}_{04} and C^{ab}_{44}; this means that these terms represent a thermoelectric effect which gives rise to a microscopic electric current.

As already noted earlier, our expression for ν^{22}_l in Eq. (3.1) can be greatly simplified by analyzing the mass dependence of the matrix elements in Eqs. (3.18) and (3.19). Expressing these in units of ω_{p2}, we find that $\Gamma^{11}_{1Q}\sim(m_2/m_1)^2$, $\Gamma^{12}_{QQ}\sim(m_2/m_1)^{3/2}$, and $\Gamma^{11}_{QQ}\sim m_2/m_1$, while Γ^{22}_{1Q} and Γ^{22}_{QQ} are of order 1. Consequently, we have from Eq. (3.1) for $m_2\ll m_1$

$$\nu^{22}_l(z)=\Gamma^{22}_{11}(z)-\frac{[\Gamma^{22}_{1Q}(z)]^2}{z+\Gamma^{22}_{QQ}(z)}+O\left(\left(\frac{m_2}{m_1}\right)^2\right). \tag{3.21}$$

For the self-motion we find after a similar analysis

$$\Gamma^{sa}_{11}(t)=-\frac{1}{m_a}\sum_{a_1a_2}(n_{a_1}n_{a_2})^{1/2}\frac{1}{6\pi^2}\int_0^\infty dk'\,k'^4\,v^{aa_1}(k')\,c^{aa_2}(k')\,C^{sa}_{00}(k't)\,C^{a_1a_2}_{00}(k't)\,, \tag{3.22}$$

$$\Gamma^{sa}_{1Q}(t)=\left(\int_0^t dt'\,Z_a(t')\right)^2\frac{1}{\beta m_a^2}\sum_{a_1a_2}(n_{a_1}n_{a_2})^{1/2}(\tfrac{1}{10})^{1/2}\,\frac{1}{2\pi^2}\int_0^\infty dk'\,k'^6\,v^{aa_1}(k')\,c^{aa_2}(k')\,C^{sa}_{00}(k't)\,C^{a_1a_2}_{00}(k't) \tag{3.23}$$

and

$$\Gamma^{sa}_{QQ}(t)=3[Z_a(t)]^2\,\Gamma^{sa}_{11}(t)+(10)^{1/2}\tfrac{22}{15}\,Z_a(t)\,\Gamma^{sa}_{1Q}(t)-\left(\int_0^t dt'\,Z_a(t')\right)^4\frac{1}{\beta^2 m_a^3}$$

$$\times\sum_{a_1a_2}(n_{a_1}n_{a_2})^{1/2}\frac{3}{20\pi^2}\int_0^\infty dk'\,k'^8\,v^{aa_1}(k')\,c^{aa_2}(k')\,C^{sa}_{00}(k't)\,C^{a_1a_2}_{00}(k't)\,. \tag{3.24}$$

We now have a closed set of equations, since the memory functions Γ^{sa} determine the self-correlation functions via the Gaussian approximation; the latter in turn yield the partial density correlation functions via the effective-field approximation. The set of equations must be solved self-consistently, as discussed in Sec. V.

If we express the partial correlation functions in the preceding equations (3.22)–(3.24) in terms of mass and charge-density fluctuations, we find that the coupling to the mass fluctuations involve the combination $\sum_{a_1} n_{a_1} v^{aa_1}$. For purely Coulombic potentials, this coupling would be identically zero, due to overall charge neutrality, and the integrals in Eqs. (3.22)–(3.24) would only contain the coupling between the self-motion of a particle and the charge fluctuations in the medium. Even with the effective potentials defined in Eqs. (1.4) and (1.5), we expect the dominant contribution to the self-motion to arise from the latter coupling. Physically, in a mass fluctuation both species move in phase, and hence, do not produce any net force acting on the self-particle, while a charge fluctuation creates an electric field which will influence the motion of the individual particle.

IV. WEAK-COUPLING LIMIT

In order to make contact with earlier work on coupled plasmas, we shall consider here the limit $\Gamma \ll 1$. The effective potentials reduce then to the bare Coulomb potential, and the direct correlation functions to their Debye-Huckel limit

$$c^{ab}(k)=-\beta v^{ab}(k)\,. \tag{4.1}$$

The various correlation functions, on the other hand, can be expressed in terms of the free-particle propagators

$$C^{ab}_{00}(kt)=\exp\left(-\frac{k^2}{2\beta m_a}t^2\right)\delta_{ab}\,, \tag{4.2}$$

$$C^{ab}_{04}(kt)=-\frac{1}{\sqrt{6}}\frac{k^2}{\beta m_a}t^2\exp\left(-\frac{k^2}{2\beta m_a}t^2\right)\delta_{ab}\,, \tag{4.3}$$

and

$$C^{ab}_{44}(kt)=\left(1-\frac{2}{3}\frac{k^2}{\beta m_a}t^2+\frac{1}{6}\frac{k^4}{(\beta m_a)^2}t^4\right)\times\exp\left(-\frac{k^2}{2\beta m_a}\right)\delta_{ab}\,, \tag{4.4}$$

which coincide with the corresponding self-parts. Inserting these expressions into our formulas for the memory functions, we obtain from Eq. (3.8)

$$\Gamma^{22}_{11}(z=0)=Z\Gamma^{3/2}\left(\frac{2}{3\pi}\right)^{1/2}\ln\frac{k_{max}}{k_{min}}\,, \tag{4.5}$$

where k_{max} and k_{min} are two cutoff wave numbers. Choosing these, in the usual way, to be the inverse Landau and Debye lengths, respectively, we obtain a Spitzer-type expression for Γ^{22}_{11}.[6,7] From Eqs. (3.18) and (3.19), we can similarily calculate the low-frequency limit of Γ^{22}_{1Q} and Γ^{22}_{QQ}:

$$\Gamma^{22}_{1Q}(z=0)=-\frac{3}{\sqrt{10}}\Gamma^{22}_{11}(z=0)\,, \tag{4.6}$$

$$\Gamma^{22}_{QQ}(z=0)=\frac{13Z+4\sqrt{2}}{10Z}\Gamma^{22}_{11}(z=0)\,. \tag{4.7}$$

Inserting these results into the expression (2.23) for the dc conductivity $\sigma=\sigma(z=0)$, we recover the well-known result[15-19]

$$\sigma=\frac{13Z+4\sqrt{2}}{4Z+4\sqrt{2}}\sigma^{(1)}\,, \tag{4.8a}$$

where

$$\sigma^{(1)}=\frac{\omega_p^2}{4\pi}\left(\frac{\rho}{\rho_1}\Gamma^{22}_{11}(z=0)\right)^{-1}=\frac{\omega_p}{4\pi}\left(\frac{3\pi}{2}\right)^{1/2}\left(\frac{\rho}{\rho_1}Z\Gamma^{3/2}\ln\frac{k_{max}}{k_{min}}\right)^{-1} \tag{4.8b}$$

is the conductivity calculated in the one Sonine polynomial approximation. In Ref. 5 it was shown how the cutoff and divergence problems arising in the standard Spitzer expression (4.8) can be overcome by an Enskog-type procedure which preserves the exact statics.

The large contribution to σ from Γ^{22}_{1Q} and Γ^{22}_{aa}, which, for $Z=1$, results in a factor 1.93, is mainly a mass effect.[15] If we consider an ionic fluid where the two species have essentially equal masses, such as a molten salt, we obtain in the

weak-coupling limit, starting from Eq. (3.1)

$$\sigma = \tfrac{59}{50}\sigma^{(1)}, \tag{4.9}$$

i.e., in this case the enhancement due to energy fluctuations results only in a factor of 1.18.

This strong dependence on the mass ratio of the terms coupling to the energy fluctuations has a simple physical interpretation. A local fluctuation of the energy will give rise to a corresponding temperature gradient, and this in turn induces a diffusion of the particles. In a plasma where $m_2 \ll m_1$, this duffusion affects only the electrons, and, therefore, results in a microscopic electric current, while in a system with equal masses, both species diffuse in the same direction, thereby preserving local charge neutrality and inducing no electric current. In a weakly coupled electron-ion plasma, the microscopic electric current due to thermoelectric effects, therefore, gives a contribution which is comparable to that arising from charge fluctuations, while in a molten salt the latter effect dominates. The simple proportionality which exists between the matrix elements in Eqs. (4.6) and (4.7) reflects the fact that in the weak-coupling limit the energy fluctuations are due to the motion of the individual particles. However, if we increase the coupling, an energy fluctuation will mainly spread out through collisions between the particles, and not through particle flow. For this reason we expect the nonlinear coupling to the energy fluctuation to become less important with increasing Γ, i.e., the numerical factors 1.93 or 1.18 should decrease for larger Γ values. For a real molten salt, which is a strongly coupled ionic fluid with $\Gamma \simeq 50$ and $m_1 \simeq m_2$,[20] the conductivity can therefore be calculated by just considering the coupling to the charge fluctuations, embodied in Γ_{11}^{22}.

For the electron self-motion, we similarly find for $\Gamma \ll 1$

$$\Gamma_{1Q}^{s2}(z=0) = -\frac{3}{2\sqrt{10}}\,\frac{4Z+\sqrt{2}}{2Z+\sqrt{2}}\,\Gamma_{11}^{s2}(z=0) \tag{4.10}$$

and

$$\Gamma_{QQ}^{s2}(z=0) = \frac{104Z+59\sqrt{2}}{40(2Z+\sqrt{2})}\,\Gamma_{11}^{s2}(z=0). \tag{4.11}$$

This gives for the electron diffusion constant

$$D_2 = \frac{104Z^2+111\sqrt{2}\,Z+59}{32Z^2+75\sqrt{2}\,Z+50}\,D_2^{(1)}, \tag{4.12a}$$

where $D_2^{(1)}$ denotes the value obtained from the first term, Γ_{11}^{s2}, in Eq. (3.4) (one Sonine polynomial approximation):

$$D_2^{(1)} = a^2\omega_{p2}\left(\frac{\pi}{3}\right)^{1/2}\left((Z\sqrt{2}+1)\Gamma^{5/2}\ln\frac{k_{\max}}{k_{\min}}\right)^{-1}. \tag{4.12b}$$

For $Z=1$, Eq. (4.12a) gives $D_2 = 1.70D_2^{(1)}$, i.e., the electron diffusion is also greatly enhanced when energy fluctuations are taken into account. When $m_1 = m_2$, we again find $D_2 = 1.18D_2^{(1)}$. The *ionic* diffusion on the other hand is largely independent of the mass ration, and the second term in Eq. (3.4) yields a factor of 1.18 both for $m_1 \gg m_2$ and $m_1 = m_2$.

V. NUMERICAL RESULTS

On the basis of the theory presented in Sec. III, we have calculated $J(t)$ and $Z_2(t)$ for a hydrogen plasma ($Z=1$) and for a carbon plasma ($Z=6$), for several values of Γ and r_s. The calculations have been performed using effective potentials both without [Eq. (1.4)] and with [Eq. (1.5)] electron symmetry effects included. In this section we confront the theoretical correlation functions with the simulation results for a hydrogen plasma.[3,4] Since the data of Refs. 3 and 4 are based on the effective pair potentials (1.4) which take no account of the Pauli principle, we have carried out additional MD simulations, including symmetry effects via the extra term (1.5) in the electron-electron potential. Two simulations were performed on a system of 64 electrons and 64 protons in a cubic volume with the usual periodic boundary conditions and Ewald summations of the interactions of one particle with the infinite array of periodic images of all other particles. The essential characteristics of these simulations are summarized in Table I. It should be noted that both in the previous work[3,4] and in the present simulations, the statistical uncertainties on D_2

TABLE I. Details of the MD simulations. Δt is the time step in the numerical integration of the equations of motion and N_t is the total number of steps in the simulation.

	Γ	r_s	T (K)	n (cm^{-3})	ω_{p2} (sec^{-1})	$\omega_{p2}\Delta t$	N_t
1st run	2	1	1.58×10^5	1.61×10^{24}	7.2×10^{16}	0.03	220 000
2nd run	0.5	1	6.3×10^5	1.61×10^{24}	7.2×10^{16}	0.02	110 000

are estimated to be 3%, while they are much larger (as much as 20%) for σ.

A. Iteration scheme

In the framework of the kinetic theory discussed in Sec. III, we have obtained the dynamical correlation functions by solving the matrix equations (B2), (B4), and (B6). For the static input quantities, we have systematically used the numerical solutions of the coupled hypernetted chain (HNC) equations, which yield excellent partial pair distribution functions compared to the MD data.[3,4] To calculate $J(t)$ and $Z_2(t)$, we need six correlation functions, C_{00}^{ab}, C_{04}^{12}, C_{04}^{22}, and C_{44}^{22}. In our approximation scheme, all dynamics are expressed in terms of the velocity ACF's $Z_1(t)$ and $Z_2(t)$. Within the characteristic times of the electronic motion, which govern the decay of $J(t)$ and $Z_2(t)$, the much slower ions behave essentially as free particles, i.e., $Z_1(t) \simeq 1$. To obtain an initial guess of $Z_1(t)$ and $Z_2(t)$, we have used the short time expansion of their memory functions $M_1(t)$ and $M_2(t)$.[27] From this initial guess we have then calculated $J(t)$ and $Z_2(t)$, and from these new values of $Z_2(t)$, we have calculated a second set of values of $J(t)$ and $Z_2(t)$, and so on. The values of $Z_1(t)$ have not been changed in this iteration scheme, since, as already pointed out, the ionic motion is practically free-particle-like within the characteristic times of the much faster electronic motion. In practice this scheme converged after only one iteration.

B. Electrical conductivity of the hydrogen plasma

We first present our results for the electric current ACF $J(t)$ of a hydrogen plasma, obtained with the potential model (1.4) (i. e., without electron symmetry effects), and compare them to the MD data of Refs. 3 and 4 based on the same effective potentials. The theoretical (full curves) and computer generated (dots) $J(t)$ curves are shown in Fig. 1 for the three states $r_s = 0.4$, $\Gamma = 0.5$, and $r_s = 1$, $\Gamma = 0.5$ and 2. The agreement between

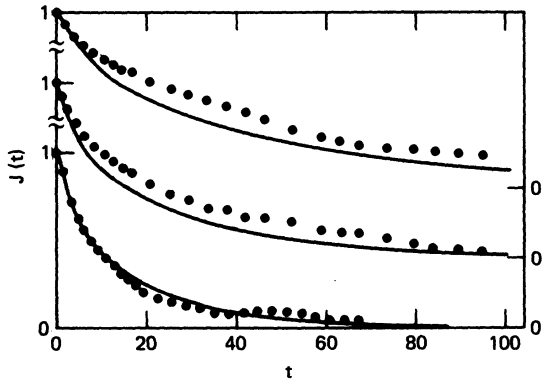

FIG. 1. Normalized electric current ACF $J(t)$ of the hydrogen plasma for, from top to bottom, $r_s = 0.4$, $\Gamma = 0.5$; $r_s = 1$, $\Gamma = 0.5$; and $r_s = 1$, $\Gamma = 2$. The full curves are our theoretical results and the dots represent the simulation results of Hansen and McDonald (Refs. 3 and 4). The time is in units of ω_{p2}^{-1} which will remain our unit of time in all subsequent figures.

our theory and the MD data is excellent for the strongest coupling ($\Gamma = 2$), while the results for the two other cases show rather large discrepancies. The corresponding values of the dc conductivity are listed in Table II. For $r_s = 1$, $\Gamma = 0.5$, the theoretical conductivity lies almost 30% below its "exact" MD value, while for the other states the agreement is better. If we had used free-particle dynamics, instead of the effective-field approximation, while including the correct statics by making the approximation

$$C_{\mu\nu}^{ab}(\vec{k}z) = C_{\mu\lambda}^{0a}(\vec{k}z)\bar{C}_{\lambda\nu}^{ab}(\vec{k}), \tag{5.1}$$

where C^{0a} denotes the free particle correlation function, the theoretical values for σ would have been reduced by 20%. The form (5.1) has the advantage of being very simple, but it violates the obvious symmetry of C^{ab} and it yields a too rapid initial decay of $J(t)$.

The large discrepancy between the theoretical results and the MD data at $\Gamma = 0.5$ may, in fact, reflect the insufficient accuracy of the effective-field approximation used in the present work to compute the C^{ab}. The calculation of Γ_{11}^{22}, for in-

TABLE II. The reduced electrical conductivity $\sigma^* = \sigma/\omega_p$ and electron self-diffusion constant $D^* = D_2/a^2\omega_{p2}$ calculated without (a) and with (b) electron symmetry effects included. MD refers to the molecular-dynamics simulation results.

		σ^* (MD)		σ^* (theory)		D_2^* (MD)		D_2^* (theory)	
r_s	Γ	(a)	(b)	(a)	(b)	(a)	(b)	(a)	(b)
0.4	0.5	3.6		3.13	3.10	12.3		12.4	5.7
1	0.5	2.15	2.55	1.57	1.45	7.2	5.1	7.0	4.85
1	2	1.1	1.5	1.12	1.27	1.23	1.11	1.31	1.05

stance, involves the difference $C_{00}^{11}C_{00}^{22} - C_{00}^{21}C_{00}^{12}$; even if the effective-field approximation yields reliable results for the three correlation functions taken separately, their combination in Γ_{11}^{22} might very well be much more sensitive to approximations.

In Fig. 2 we illustrate the time dependence of the memory function $M_J(t)$ (full curve) in the state $r_s = 1$, $\Gamma = 2$. It is seen that $M_J(t)$ exhibits a rapid initial decay followed by a long-lived oscillatory part. These oscillations reflect the coupling to the charge-density fluctuations. In the same figure we also show the contributions to $M_J(t)$ from $(\rho/\rho_1)\,\Gamma_{11}^{22}$ (dashed curve) and from the coupling to the energy fluctuations, i.e., the time dependence of $-(\rho/\rho_1)[\Gamma_{1Q}^{22}(z)]^2/[z + \Gamma_{QQ}^{22}(z)]$ (dots). Since it takes some time to build up a diffusion current, this latter part starts rather late, but once it has built up, it decays slowly. The relative contributions of $I_{1Q}^{22}(z=0)$ and $I_{QQ}^{22}(z=0)$ are given in Table III, and these values should be compared to the weak-coupling results $\Gamma_{1Q}^{22}(z=0) = -0.95\,\Gamma_{11}^{22}(z=0)$ and $\Gamma_{QQ}^{22}(z=0) = 1.86\Gamma_{11}^{22}(z=0)$. For the state $r_s = 1$, $\Gamma = 2$ we find $\sigma = 1.57\sigma^{(1)}$, i.e., the factor 1.93, valid for weak coupling, has decreased significantly with increasing Γ. For the other two states, corresponding to $\Gamma = 0.5$, the oscillations in $M_J(t)$ are less pronounced. The contribution from the energy fluctuations develops a very long-lived negative plateau and this increases the relative importance of this term.

In Fig. 3 we show an example of the real and imaginary parts of the ac conductivity obtained from the theoretical (full and dashed curves) and MD (dots and squares) results for $J(t)$ [cf. Eq. (2.7)]. The oscillations in the MD results are most probably due to numerical truncation errors and statistical uncertainties.

The results for the electrical conductivity obtained when electron symmetry effects are included are also summarized in Tables II and III, and in Fig. 4. The theoretical values for σ are not drastically changed upon inclusion of the symmetry term (1.5) in the effective potential, in agreement with the MD data, but the various matrix elements

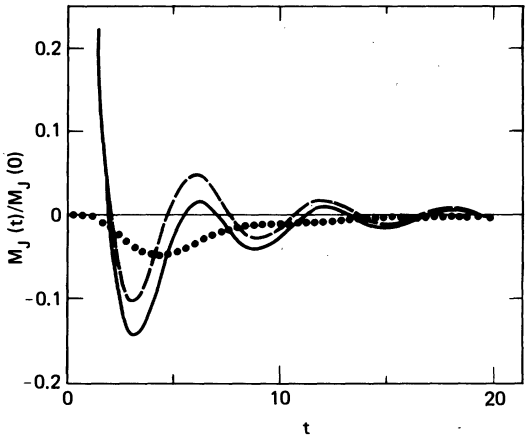

FIG. 2. Normalized memory function $M_J(t)/M_J(t=0)$ versus time for $r_s = 1$, $\Gamma = 2$. The full curve represents the total memory function, the dashed curve is the contribution from $(\rho/\rho_1)\Gamma_{11}^{22}(t)$, and the dotted curve shows the time dependence of $-(\rho/\rho_1)[\Gamma_{1Q}^{22}(z)]^2/[z + \Gamma_{QQ}^{22}(z)]$.

are affected rather strongly. The large increase in the area of Γ_{QQ}^{22} will reduce the importance of the coupling to the energy fluctuations. The reason for this behavior is that the additional repulsion between electrons, due to the Pauli principle, will reduce the electron diffusion, and thereby the electric diffusion current. However, at the same time, the stronger repulsion between electrons will tend to decrease the number of electrons around any given proton; the system becomes then effectively more polarized, whereby charge fluctuations are enhanced. The resulting contribution to σ is increased and partly compensates the reduction of the coupling to the energy fluctuations. In fact, in the most degenerate case ($r_s = 1$, $\Gamma = 2$), this latter effect dominates the former, leading to a slight increase in σ.

C. Electron self-diffusion in the hydrogen plasma

Our results for the electron velocity ACF are shown in Figs. 5 (without electron symmetry ef-

TABLE III. Relative contribution of the coupling to the energy fluctuations, to the areas of the memory functions for the conductivity and self-motion in the hydrogen plasma. (a) and (b) refer again to calculations without and with electron symmetry effects included.

r_s	Γ	$\Gamma_{1Q}^{22}(z=0)/\Gamma_{11}^{22}(z=0)$		$\Gamma_{QQ}^{22}(z=0)/\Gamma_{11}^{22}(z=0)$		$\Gamma_{1Q}^{s2}(z=0)/\Gamma_{11}^{s2}(z=0)$		$\Gamma_{QQ}^{s2}(z=0)/\Gamma_{11}^{s2}(z=0)$	
		(a)	(b)	(a)	(b)	(a)	(b)	(a)	(b)
0.4	0.5	−0.93	−0.88	2.00	4.69	−0.64	−0.39	1.62	1.79
1	0.5	−0.90	−0.87	1.87	2.51	−0.67	−0.55	1.55	1.59
1	2	−0.84	−0.83	1.95	2.93	−0.61	−0.43	1.67	1.92

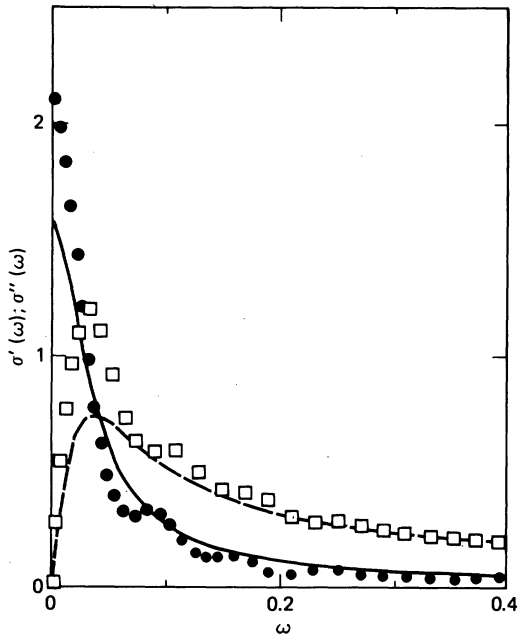

FIG. 3. Real $[\sigma'(\omega)]$ and imaginary $[\sigma''(\omega)]$ parts of the ac conductivity $\sigma(z=-i\omega)$ vs ω of a hydrogen plasma for $r_s=1$, $\Gamma=0.5$. The full and dashed curves are $\sigma'(\omega)$ and $\sigma''(\omega)$, respectively, based on our theory, while the dots and squares represent the simulation data (Refs. 3 and 4) for $\sigma'(\omega)$ and $\sigma''(\omega)$. $\sigma'(\omega)$ and $\sigma''(\omega)$ are in units of ω_{p2}.

fects) and 6 (including electron symmetry effects) for the same states as above. The agreement with the MD results (dots) is nearly perfect, and the values of the diffusion constant D_2, listed in Table II, agree within a few percent with the MD values. The time dependence of $Z_2(t)$ is rather simple, compared to the complex behavior of $J(t)$, and is rather accurately represented by an exponential function.[4] In Fig. 7 we show the time dependence

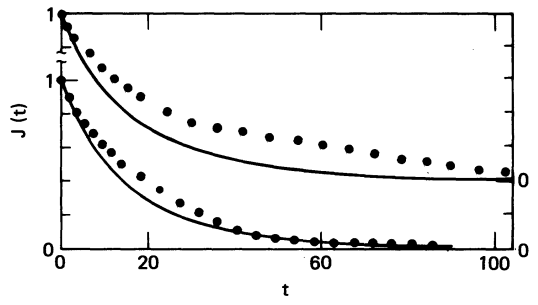

FIG. 4. $J(t)$ for the hydrogen plasma versus t, for $r_s=1$, $\Gamma=0.5$, and $\Gamma=2$, when electron symmetry effects are included in the effective pair potential; the full curve represents the theoretical results, and the dots the simulation data.

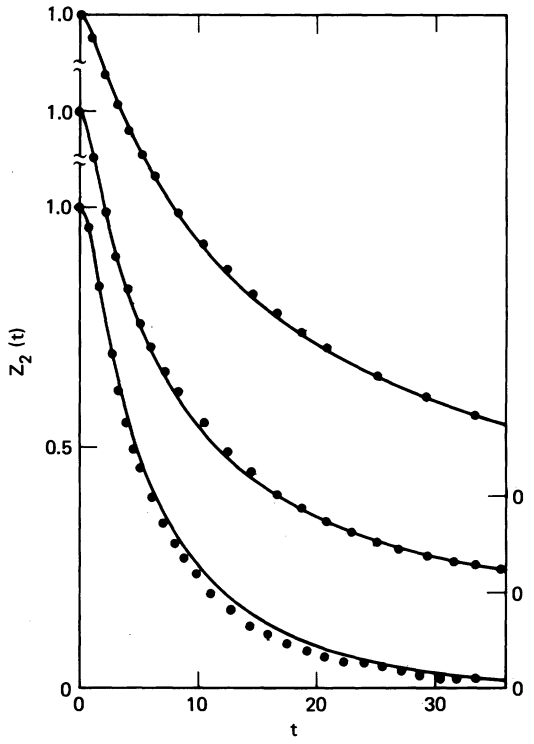

FIG. 5. Electron velocity ACF, $Z_2(t)$, versus time in the hydrogen plasma without electron symmetry effects and for, from top to bottom, $r_s=0.4$, $\Gamma=0.5$; $r_s=1$, $\Gamma=0.5$, and $r_s=1$, $\Gamma=2$. The full curves display our theoretical results and the dots the simulation data (Refs. 3 and 4).

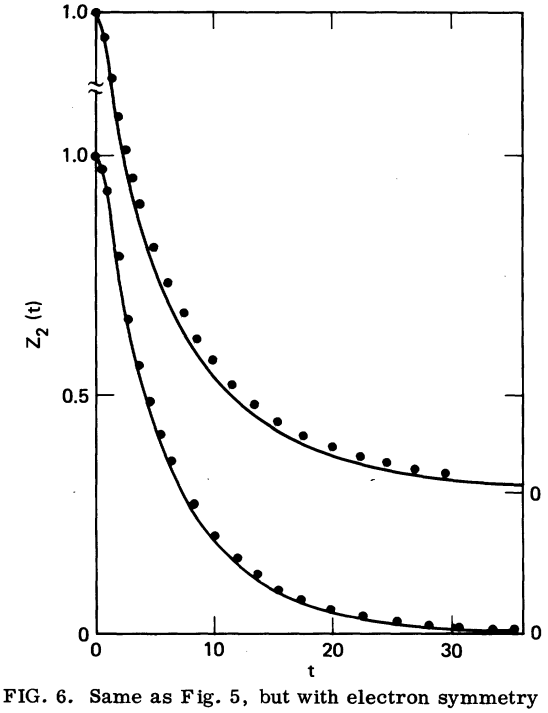

FIG. 6. Same as Fig. 5, but with electron symmetry effects included, and for $r_s=1$, $\Gamma=0.5$, and 2.

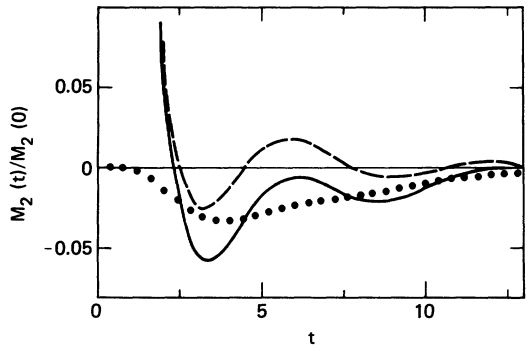

FIG. 7. Normalized memory function $M_2(t)/M_2(0)$ (full curve) versus time for $r_s=1$, $\Gamma=2$ for a hydrogen plasma without electron symmetry effects. The dashed curve shows $\Gamma_{11}^{s2}(t)$ and the dotted curve shows the time dependence of $-[\Gamma_{1Q}^{s2}(z)]^2/[z+\Gamma_{QQ}^{s2}(z)]$.

of $M_2(t)$ for $r_s=1$, $\Gamma=2$ (without electron symmetry effects). The oscillating tail reflects again the coupling of the single-particle motion to the charge-density fluctuations in the medium. The dashed curve shows the contribution from Γ_{11}^{s2} and the dotted curve, the contribution corresponding to $-[\Gamma_{1Q}^{s2}(z)]^2/[z+\Gamma_{QQ}^{s2}(z)]$. The overall qualitative behavior is similar to that found for $M_J(t)$ above. The relative contributions to the area of $M_2(t)$ from Γ_{1Q}^{s2} and Γ_{QQ}^{s2} are also given in Table III, and should be compared to the weak-coupling results derived in Sec. IV, $\Gamma_{1Q}^{s2}(z=0)=-0.75\Gamma_{11}^{s2}(z=0)$ and $\Gamma_{QQ}^{s2}(z=0)=1.37\Gamma_{11}^{s2}(z=0)$.

A possible reason why our theory works much better for $Z_2(t)$ than for $J(t)$ is that the matrix elements in Eqs. (3.22)–(3.24) involve essentially the combination $C_{\mu\nu}^{s2}(kt)C_{zz}(kt)$, with μ, $\nu=0$, and 4. Since the effective-field approximation yields rather accurate results for C_{zz},[27] our calculation of Γ_{11}^{s2}, Γ_{1Q}^{s2}, and Γ_{QQ}^{s2} is probably more accurate than the corresponding elements for the conductivity, which involves *differences* of correlation functions.

The effect on the diffusion constant upon including symmetry effects is rather large, as seen from Table II, and leads to a reduction of D_2 due to the increase of the electron-electron collision rate. The various matrix elements are also affected, but the qualitative time dependence of $M_2(t)$ is similar to that shown in Fig. 7.

D. Long-wavelength limit of the dynamical charge structure factor

The function $J(z)$ contains all the information on the dynamical charge structure factor

$$S_{zz}(k\omega)=\frac{1}{\pi}\mathrm{Re}C_{zz}(k,z=-i\omega) \tag{5.2}$$

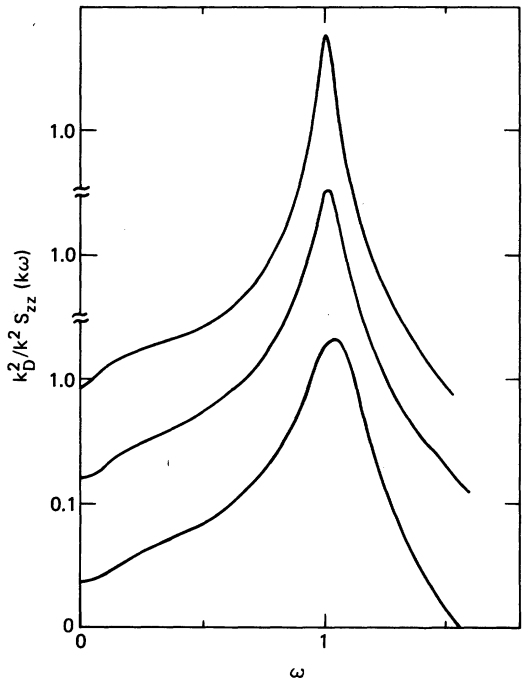

FIG. 8. $\mathrm{Lim}_{k\to 0}(k_D^2/k^2)S_{zz}(k,\omega)$ vs ω for a hydrogen plasma and the states, from top to bottom, $r_s=0.4$, $\Gamma=0.5$, $r_s=1$, $\Gamma=0.5$, and $r_s=1$, $\Gamma=2$. The vertical scale is logarithmic and in units of ω_{p2} and ω is in units of $\omega_{p2}\simeq\omega_p$.

in the limit $k\to 0$. Using Eqs. (2.20), (2.24), and the "perfect screening" condition

$$\lim_{k\to 0}\frac{k_D^2}{k^2}S_{zz}(k)=1 \tag{5.3}$$

we arrive at the desired result

$$\lim_{k\to 0}\frac{k_D^2}{k^2}C_{zz}(k,z)=\frac{z+M_J(z)}{z^2+\omega_p^2+zM_J(z)}. \tag{5.4}$$

It follows from Eqs. (5.3) and (5.4) that the long wavelength charge fluctuation spectrum $S_{zz}(0,\omega)$ exhibits two conjugate peaks around $\pm\omega_p$. The *damping* of the plasma oscillations is determined by the memory function M_J, which also introduces a slight frequency *shift* relative to the plasma frequency ω_p.[11,28] In Fig. 8 we show the theoretical results for $\lim_{k\to 0}(k_D^2/k^2)S_{zz}(k,\omega)$ when no electron symmetry effects are included in the effective potential. As expected the dominant feature is a very sharp resonance shifted slightly *above* ω_p. This shift is largest for $r_s=1$, $\Gamma=2$, where it reaches 4%, while for the less strongly coupled states it is only of the order of 1%. The inclusion of electron symmetry effects has a negligible effect on the spectra.

A sizable shift of the plasma frequency, due to interspecies collisions (resistivity) had already

been established in Ref. 4 on the basis of a simple memory function analysis[29] and a prescription for the relaxation times due to Lovesey.[30] This resulted in much larger frequency shifts than those predicted here. The origin of this increased shift can be traced back to the fact that the Lovesey model underestimates the dc conductivity σ by more than a factor of 2. This finding confirms the failure of the Lovesey prescription in the limit $k \to 0$, where it also yields an infinite viscosity, whereas it describes the charge fluctuations very well for intermediate and large wave numbers.[4]

E. Results for the carbon plasma

In order to investigate the Z dependence of our results, we have also made some calculations for a carbon plasma ($Z = 6$). The results for $J(t)$ are shown in Fig. 9. Since the higher valence of the ions leads to a stronger attraction of the electrons, the plasma is locally more neutral and the conductivity is reduced. From Eq. (4.8) we find that in the weak-coupling limit $\sigma = 2.82\sigma^{(1)}$ for $Z = 6$, i.e., the relative importance of the coupling to energy fluctuations is increased, but at the same time $\sigma^{(1)} \sim 1/Z$ and the total effect is a reduction of σ, practically by a factor $\frac{1}{6}$ compared to the conductivity of the hydrogen plasma. For the electron diffusion we find from (4.12a) that $D_2 = 2.58 D_2^{(1)}$. The enhanced ion-electron attraction reduces the relative importance of electron-electron collisions and as a result the factor $Z\sqrt{2}$ in (4.12b) dominates over 1. The total effect is to reduce the electron diffusion constant by approximately a factor of 2 compared with the hydrogen plasma. The results for $Z_2(t)$ are shown in Fig. 10, and the values of σ and D_2 are listed in Tabel IV. It should be noted that the two last states in Table IV have a temperature

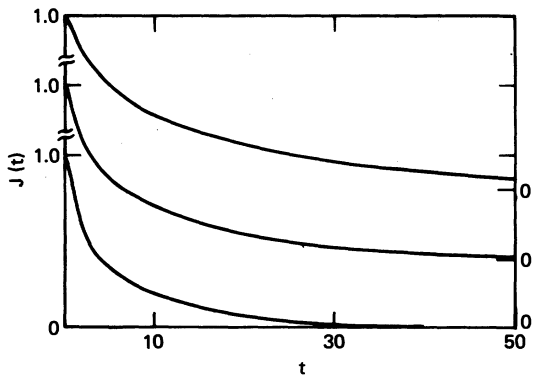

FIG. 9. $J(t)$ versus time for the carbon plasma and the three states, from top to bottom, $r_s = 0.4$, $\Gamma = 0.1$, 0.2, and 0.5.

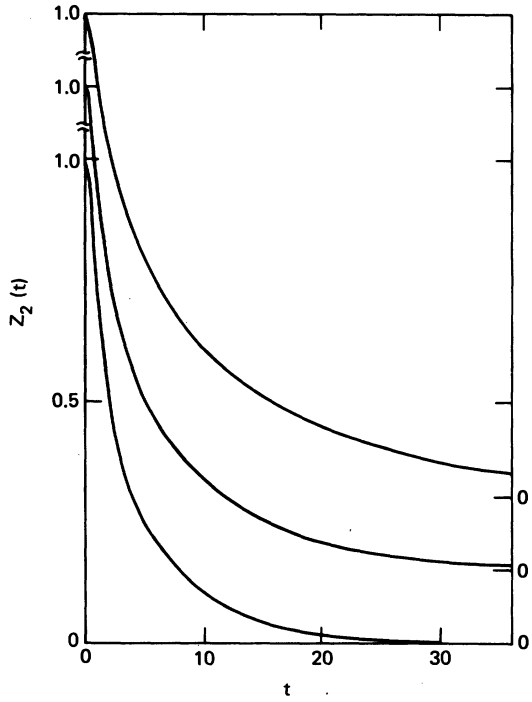

FIG. 10. $Z_2(t)$ versus time for the carbon plasma and the same states as in Fig. 10.

lower than the ionization temperature ($T \simeq 5.7 \times 10^6$ K) for an isolated carbon atom. At high density ($r_s < 1$) screening reduces the Coulomb attraction and the ionization energy for a dense C plasma is lower. However, some recombination may occur for those states, and this cannot be described in purely classical terms.

VI. DISCUSSION

The present microscopic theory for the calculation of the electric current and velocity AC F's in a strongly coupled ion-electron plasma yields results in overall satisfactory agreement with the MD simulation data. The remaining discrepancies between the theoretical and simulation results for $J(t)$ are most likely due to the input values for the dynamical density correlation func-

TABLE IV. Theoretical results for the carbon plasma, based on the potential model including electron symmetry effects.

r_s	Γ	n (cm^{-3})	T (K)	ω_p (sec^{-1})	σ^*	D_2^*
0.2	0.2	2.01×10^{26}	7.9×10^6	8.02×10^{17}	1.36	11.54
0.4	0.1	2.52×10^{25}	7.9×10^6	2.83×10^{17}	1.24	32.72
0.4	0.2	2.52×10^{25}	3.95×10^6	2.83×10^{17}	0.74	9.85
0.4	0.5	2.52×10^{25}	1.58×10^6	2.83×10^{17}	0.48	2.69

tions, which are based on the effective-field approximation. Another origin of the remaining discrepancy could be the possible importance of other nonlinear couplings for intermdeiate Γ values. Additional couplings to energy fluctuations will, for instance, occur through close collisions between particles. The inclusion of such effects requires an even more elaborate microscopic theory.[21,32]

The fundamental assumption in this as well as previous[3,4,5] work is that in a weakly degenerate (or semiclassical) plasma, quantum effects, which come into play only for particle separations $r \lesssim \lambda_{ab}$, can be reasonably well accounted for by using a set of *effective* pair potentials in the framework of *classical* statistical mechanics. Moreover, these effective potentials are chosen to be identical to their low-density limit.[7,8] At present the consequences of this basic assumption can only be tested by examining the sensitivity of various correlation functions to variations of the effective potentials. For that reason we have systematically carried out our calculations for two potential models, one without and one including electron symmetry effects embodied in the Pauli repulsion term (1.5). A comparison of both sets of results shows that the long wavelength *collective* motions [reflected in the functions $J(t)$ or $S_{zz}(k=0,\omega)$] are hardly affected by details of the short-range part of the effective potentials, while the *single-particle* motion, and in particular D_2, is much more sensitive to changes in these effective potentials.

ACKNOWLEDGMENTS

The interest and collaboration of Marc Baus in the early stages of this work has been very stimulating and helpful. L.S. acknowledges the support of the Commissariat a l'Energie Atomique through the grant of a Joliot-Curie fellowship. J.P.H. is indebted to B.J. Alder and H.E. DeWitt for their hospitality at the Lawrence Livermore Laboratory, where part of this work was initiated. J.P.H. and E.L.P. acknowledge the support of NATO Research Grant 1890. This work was performed under the auspices of the U.S. Department of Energy and by the Lawrence Livermore National Laboratory under Contract No. W-7405-Eng-48.

APPENDIX A

Here we give some details of the derivation of (3.7) starting from (3.5). In order to preserve the initial value of Γ^{ab} we extract the initial value of G, denoted by $\tilde{G}$, by using the identity

$$G = G\tilde{G}^{-1}\tilde{G} = \tilde{G}\tilde{G}^{-1}G \,. \tag{A1}$$

Except for the initial value our approximations should preserve the detailed balance condition (3.3) which reflects the microscopic reversibility inherent in G,

$$G(12;34t) = G(34;12-t) \,. \tag{A2}$$

An approximation for G which satisfies both conditions, and which will be employed here, is[22]

$$G = \tfrac{1}{2}(\tilde{G}\tilde{G}_D^{-1}G_D + G_D\tilde{G}_D^{-1}\tilde{G}) \,. \tag{A3}$$

Inserting (A3) into (3.5) we obtain the combination $\tilde{G}\nabla V$ and $\nabla V\tilde{G}$, which can be expressed in terms of the static pair and triple distribution functions. Since the latter is not known we make the additional approximation[21]

$$\sum_{a_2}\int d4\,\tilde{G}^{aa_1;ba_2}(12;34)\vec{\nabla}_{r_3}v^{ba_2}(\vec{r}_3-\vec{r}_4) \simeq -\frac{1}{\beta}\sum_{a_2}\int d4\,\tilde{G}_D^{aa_1;ba_2}(12;34)\vec{\nabla}_{r_3}c^{ba_2}(\vec{r}_3-\vec{r}_4) \,, \tag{A4}$$

and analogously for $\nabla V\tilde{G}$, in (A4) c^{ab} denotes the partial direct correlation function. Inserting (A3) with (A4) into (3.5) gives (3.7).

APPENDIX B

In this appendix we give additional details concerning the calculation of the correlation functions needed in the mode-coupling expressions for the memory functions. We recall that our starting point is the effective-field approximation embodied in Eq. (3.17). In this approximation the correlation functions $C^{ab}_{\mu\nu}$ are expressed in terms of their self-parts and the static structure factors. The self-correlation functions can be expanded as follows:

$$C^{sa}_{\mu\nu}(\vec{k}t) = n_a\langle H^a_\mu(\vec{P}_{1a}(t))\exp[-i\vec{k}\cdot\vec{r}_{1a}(t)]\exp[i\vec{k}\cdot\vec{r}_{1a}(0)]H^a_\nu(\vec{P}_{1a}(0))\rangle$$
$$= n_a\sum_{n=0}^{\infty}\frac{1}{n!}\left(\frac{-ik}{m_a}\right)^n\int_0^t dt_1\cdots\int_0^t dt_n\langle H^a_\mu(\vec{p}_{1a}(t))\hat{k}\cdot\vec{p}_{1a}(t_1)\cdots\hat{k}\cdot\vec{p}_{1a}(t_n)H^a_\nu(\vec{p}_{1a}(0))\rangle \,. \tag{B1}$$

To obtain a closed expression for C^{sa} we make use of the "Gaussian approximation" whereby each statistical average in Eq. (B1) is approximated by all possible pairings of the momentum variables. Conse-

quently, all dynamics in this approximation is given in terms of the velocity ACF $Z_a(t)$.

Taking $\mu=\nu=0$ in Eq. (3.17) we obtain

$$C_{00}^{ab}(kz)+[zC_{00}^{sa}(kz)-1]\sum_{a_1}(n_a n_{a_1})^{1/2}c^{aa_1}(k)C_{00}^{a_1 b}(kz)=C_{00}^{sa}(kz)S^{ab}(k)\,, \tag{B2}$$

where we have used the continuity equation to express C_{01}^{sa} in terms of C_{00}^{sa} and $\tilde{C}_{\lambda 0}^{ab}(k)=S^{ab}(k)\delta_{\lambda 0}$. From Eq. (B1) we obtain the familiar expression for the self-density ACF:

$$C_{00}^{sa}(k,t)=\exp\left(-\frac{k^2}{\beta m_a}\int_0^t dt'(t-t')Z_a(t')\right). \tag{B3}$$

This expression is then inserted into Eq. (B2) which is a matrix equation for the three unknown functions $C_{00}^{11}, C_{00}^{12}=C_{00}^{21}$, and C_{00}^{22}.

In a similar manner we obtain equations for the matrix elements C_{04}^{ab} in the form

$$C_{04}^{ab}(kz)+[zC_{00}^{sa}(kz)-1]\sum_{a_1}(n_a n_{a_1})^{1/2}c^{aa_1}(k)C_{04}^{a_1 b}(kz)=C_{04}^{sa}(kz)\delta_{ab}\,, \tag{B4}$$

where, from Eq. (B1) (Ref. 31):

$$C_{04}^{sa}(k,t)=-\frac{k^2}{\sqrt{6}\,\beta m_a}\left(\int_0^t dt' Z_a(t')\right)^2 C_{00}^{sa}(kt)\,. \tag{B5}$$

The corresponding functions C_{40}^{ab} follow directly from the symmetry relation

$$C_{40}^{ab}(k,t)=C_{04}^{ba}(k,t)\,,$$

which is a direct consequence of the definition (2.8) and can also be verified from Eq. (3.17). For C_{44}^{ab} we find

$$C_{44}^{ab}(kz)+zC_{40}^{sa}(kz)\sum_{a_1}(n_a n_{a_1})^{1/2}c^{aa_1}(k)C_{04}^{a_1 b}(kz)=C_{44}^{sa}(kz)\delta_{ab}\,, \tag{B6}$$

with[31]

$$C_{44}^{sa}(kt)=\left[[Z_a(t)]^2-\frac{2}{3}\left(\frac{k^2}{\beta m_a}\right)Z_a(t)\left(\int_0^t dt' Z_a(t')\right)^2+\frac{1}{6}\left(\frac{k^2}{\beta m_a}\right)^2\left(\int_0^t dt' Z_a(t')\right)^4\right]C_{00}^{sa}(kt)\,. \tag{B7}$$

The other correlation functions appearing in the mode-coupling expressions can, as a consequence of the Gaussian approximation, now be expressed in terms of C_{04}^{ab} and C_{44}^{ab}; we find

$$C_{08}^{ab}(kt)=\sqrt{6}\,\hat{k}^\varepsilon\hat{k}^\beta C_{04}^{ab}(kt)\,, \tag{B8}$$

$$C_{48}^{ab}(\vec{kt})=\sqrt{6}\,\hat{k}^\varepsilon\hat{k}^\beta C_{44}^{ab}(kt)+\sqrt{6}\,(\tfrac{1}{3}\delta_{\beta\varepsilon}-\hat{k}^\varepsilon\hat{k}^\beta)[Z_a(t)]^2 C_{00}^{sa}(kt)\delta_{ab}\,, \tag{B9}$$

and

$$\begin{aligned}C_{\alpha\beta}^{ab}(kt)=6(\hat{k}^\varepsilon)^2\hat{k}^\alpha\hat{k}^\beta C_{44}^{ab}(kt)+\Big[&[\delta_{\alpha\beta}+\delta_{\alpha\varepsilon}\delta_{\beta\varepsilon}-6(\hat{k}^\varepsilon)^2\hat{k}^\alpha\hat{k}^\beta]\,[Z_a(t)]^2\\&-[\hat{k}^\alpha\hat{k}^\beta+\delta_{\beta\varepsilon}\hat{k}^\alpha\hat{k}^\varepsilon+\delta_{\alpha\varepsilon}\hat{k}^\beta\hat{k}^\varepsilon+\delta_{\alpha\beta}(\hat{k}^\varepsilon)^2-4(\hat{k}^\varepsilon)^2\hat{k}^\alpha\hat{k}^\beta]\\&\times\left(\frac{k^2}{\beta m_a}\right)Z_a(t)\left(\int_0^t dt' Z_a(t')\right)^2\Big]C_{00}^{sa}(kt)\delta_{ab}\,.\end{aligned} \tag{B10}$$

This set of equations yields all of the required correlation functions in terms of the velocity ACF's. We now have to solve the matrix equations (B2), (B4), and (B6). Actually, we only need the functions C_{04}^{12} and C_{04}^{22} from Eq. (B4) and C_{44}^{22} from Eq. (B6) in order to calculate the matrix elements Γ_{1Q}^{22} and Γ_{QQ}^{22}.

---

*Permanent address: Institute of Theoretical Physics, Chalmers University of Technology, S41296 Göteborg, Sweden.

†Equipe Associee au CNRS.

[1] *Strongly Coupled Plasmas*, edited by G. Kalman (Plenum, New York, 1978).

[2] Laser Plasma Interactions, edited by J. J. Sanderson and R. A. Cairns, Proceedings of the 20th Scottish Universities Summer School in Physics, 1979 (unpublished).

[3]J. P. Hansen and I. R. McDonald, Phys. Rev. Lett. 41, 1379 (1978).
[4]J. P. Hansen and I. R. McDonald, Phys. Rev. A (in press).
[5]M. Baus, J. P. Hansen, and L. Sjögren (unpublished).
[6]L. Spitzer, *Physics of Fully Ionized Gases* (Interscience, New York, 1956).
[7]C. Deutsch, Phys. Lett. A60, 317 (1977).
[8]C. Deutsch, M. M. Gombert, and H. Minoo, Phys. Lett. 66A, 381 (1978); 72A, 481 (1979); H. Minoo, M. M. Gombert, and C. Deutsch (unpublished).
[9]G. F. Mazenko, Phys. Rev. A 9, 360 (1974); G. F. Mazenko and S. Yip, in *Statistical Mechanics, Part B*, edited by B. J. Berne (Plenum, New York, 1977).
[10]J. I. Castresana, G. F. Mazenko, and S. Yip, Ann. Phys. (N.Y.) 103, 1 (1977); J. R. Mehaffey and R. I. Cukier, Phys. Rev. A 17, 1181 (1978).
[11]M. Baus, Physica Utrecht 88A, 319 (1977); 88A, 336 (1977); 88A, 591 (1977).
[12]M. Parrinello and M. P. Tosi, Rev. Nuovo Cimento 2, 1 (1979).
[13]S. Chapman and T. G. Cowling, *The Mathematical Theory of Non-Uniform Gases* (Cambridge University Press, London, 1939).
[14]D. Forster and P. C. Martin, Phys. Rev. A 2, 1575 (1970).
[15]T. G. Cowling, Proc. R. Soc. London 183, A453 (1945).
[16]R. Landshoff, Phys. Rev. 76, 904 (1949); 82, 442 (1951).
[17]L. Spitzer and R. Härm, Phys. Rev. 89, 997 (1953).
[18]B. B. Robinson and I. B. Bernstein, Ann. Phys. (N.Y.) 18, 110 (1962).
[19]R. H. Williams and H. E. DeWitt, Phys. Fluids 12, 2326 (1969).
[20]J. P. Hansen and I. R. McDonald, Phys. Rev. A 11, 2111 (1975).
[21]L. Sjögren, Phys. Rev. A 22, 2866 (1980).
[22]J. Wallenborn and M. Baus, Phys. Rev. A 18, 1737 (1978).
[23]S. K. Mitra and S. Sjodin, J. Phys. C 11, 2655 (1978).
[24]P. V. Giaquinta, M. Parinello, and M. P. Tosi, Phys. Chem. Liq. 5, 305 (1976).
[25]W. C. Kerr, Phys. Rev. 174, 316 (1968).
[26]B. Bernu, J. Stat. Phys. 21, 447 (1979).
[27]L. Sjögren and J. P. Hansen (unpublished).
[28]M. Baus, Phys. Rev. Lett. 40, 793 (1978).
[29]M. C. Abramo, M. Parrinello, and M. P. Tosi, J. Phys. C 7, 4201 (1974).
[30]S. W. Lovesey, Phys. Lett. 36A, 413 (1971).
[31]S. Sjödin and A. Sjölander, Phys. Rev. A 18, 1723 (1978).
[32]L. Sjögren and A. Sjölander, J. Phys. C 12, 4369 (1979).